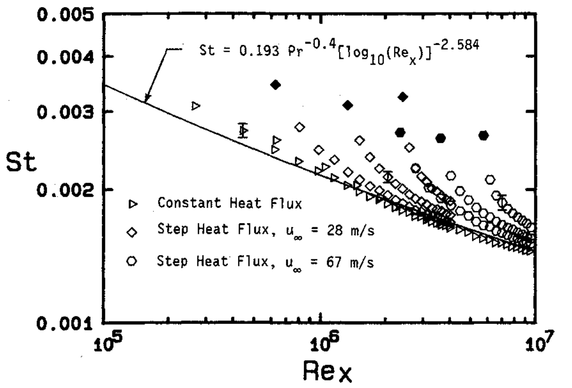

Fig. 1 Summary of the Stanton number data for the constant heat flux boundary condition and the unheated starting length cases.

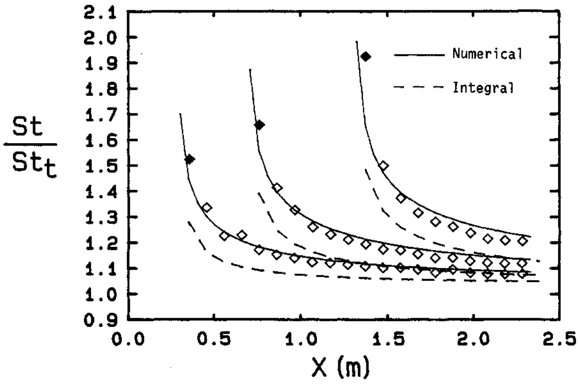

Fig. 2 Comparison of the data with the solutions for $u_\infty = 28$ m/s.

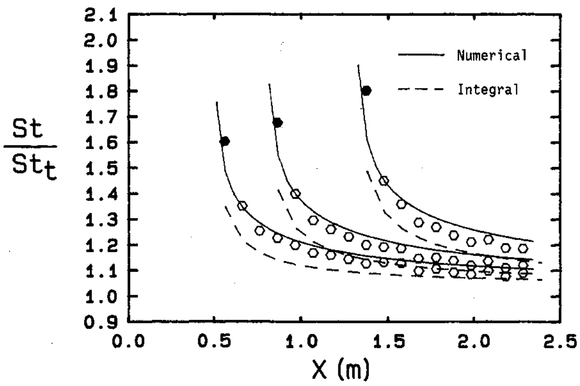

Fig. 3 Comparison of the data with the solutions for $u_\infty = 67$ m/s.

temperature profiles. Therefore, they should be viewed as asymptotic cases in which the boundary layers have become well developed.

References

[1]Reynolds, W. C., Kays, W. M., and Kline, S. J., "Heat Transfer in the Turbulent Incompressible Boundary Layer, Parts I, II, and III," NASA Memo 12-1-58W, 12-2-58W, and 12-3-58W, 1958.

[2]Coleman, H. W., Hosni, M. H., Taylor, R. P., and Brown, G. B., "Smooth Wall Qualification of a Turbulent Heat Transfer Test Facility," TFD-88-2, Mechanical and Nuclear Engineering Department, Mississippi State University, Mississippi State, MS, 1988.

[3]Love, P., Taylor, R. P., Coleman, H. W., and Hosni, M. H., "Effects of Thermal Boundary Condition on Heat Transfer in the Turbulent Incompressible Flat Plate Boundary Layer," Mechanical and Nuclear Engineering Department, Mississippi State University, Mississippi State, MS, TFD-88-3, 1988.

[4]Gatlin, B., "An Instructional Computer Program for Computing the Steady, Compressible, Turbulent Flow of an Arbitrary Fluid Near a Smooth Wall," MS Thesis, Mechanical and Nuclear Engineering Department, Mississippi State University, Mississippi State, MS, 1983.

Thermal Correlation of Natural Convection in Bottom-Cooled Cylindrical Enclosures

Shou-Shing Hsieh*
National Sun Yat-Sen University,
Kaohsiung, Taiwan, Republic of China

Introduction

IN spite of the importance of convective heat transfer in vertical cylindrical enclosures in many practical applications, very few basic studies have been conducted on this system. In Refs. 1-4, one finds that the phenomenon can exist primarily in one of two exteme configurations: 1) a fluid layer heated from below and 2) a fluid layer heated from the side.

Work on the fluid layer heated from top and/or side walls has received rather limited attention as either the experimental study of turbulent natural convection or with rectangular enclosure being the only geometry considered. In fact, the technical application of this study is important to the performance assessment of a solar storage tank. In a series of papers, Yin et al.[5] and Huang[6] experimentally investigated this problem using water and 20 CS Silicone oil as the working media for different aspect ratios of $0.2 \leq H/R \leq 2.0$ and Prandtl numbers of $3 \leq Pr \leq 250$. For numerical study, the related problem of natural convection in a differentially heated corner region of a rectangular enclosure was investigated recently by Kimura and Bejan.[7] Their results show that a unicellular motion exists and migrates toward the corner as the Ra increases.

As stated earlier, the published literature is primarily restricted to the experimental study of either turbulent natural convection or rectangular enclosures. Most recently, Huang and Hsieh[8] investigated the natural convection heat transfer in a cylindrical enclosure cooled from below. There is, however, no reported information on the heat-transfer behavior in cylindrical enclosures of differing aspect ratios. Such a situation is analyzed here. This paper reports on a two-dimensional numerical simulation of buoyance-driven flows, with Prandtl numbers of the working fluid 1, 10, 100, and 200, within vertical cylindrical enclosures of differing aspect ratios (height to radius) of 0.5, 1, and 2 that are cooled from below. It is recognized that the simulation of the present problem is bound to exhibit a certain degree of three dimensionality and unsteadiness. The investigations of Figliola[9] and Kimura and Bejan[7] might be helpful in this regard, providing this bifurcation. With the side wall insulated, the top wall was cooled and the bottom wall heated in the work of Figliola.[9] The resulting flow was two-dimensional until Rayleigh numbers larger than 5×10^4 were imposed, at which point the stable single toroid broke down into three-dimensional motion. For a rectangular

Received Nov. 7, 1988; revision received March 21, 1989.

*Professor, Department of Mechanical Engineering. Member AIAA.

cavity, Kimura and Bejan[7] reported the result of laminar natural convection up to a Rayleigh number of 10^7. In this study, it can be recognized that a more stable flow configuration exists as compared with that of Figliola.[9] The maximum Rayleigh number investigated was 10^6 and, therefore, the assumption of two-dimensional flow is not unrealistic. The steady-state results presented here evolved from a time-dependent calculation scheme. In addition, a scale analysis is presented and compared with the results from the numerical computations.

Mathematical Formulation and Scale Analysis

In this study a Boussinesq fluid is considered. The natural convection motion is assumed to be laminar and two-dimensional. The physical situation to be considered is shown in Fig. 1. The governing partial differential equations involve the conservation of mass, momentum, and energy, which are nondimensionalized using the following quantities:

$$\epsilon=\frac{r}{R}, \quad \eta=\frac{z}{R}, \quad Gr=\frac{g\beta\Delta TR^3}{\nu^2}$$

$$U=\frac{uR}{\nu}, \quad V=\frac{VR}{\nu}, \quad Pr=\frac{\nu}{\alpha}$$

$$p^*=\frac{p}{(\nu^2/R)\rho}, \quad Ra=GrPr$$

$$\theta=\frac{T-T_L}{T_H-T_L}$$

Here r and z are the radial and axial coordinates, R and H are the radius and height of the cylinder, ν is the kinematic viscosity, and α is the thermal diffusivity. Subscripts H and L, respectively, denote the state of temperature of the boundary.

The resulting equations are

$$\frac{\partial U}{\partial \epsilon}+\frac{U}{\epsilon}+\frac{\partial V}{\partial \eta}=0 \tag{1}$$

$$\frac{\partial U}{\partial \tau}+U\frac{\partial U}{\partial \epsilon}+V\frac{\partial U}{\partial \eta}=-\frac{\partial P^*}{\partial \epsilon}+\frac{\partial^2 U}{\partial \epsilon^2}+\frac{1}{\epsilon}\frac{\partial^2 U}{\partial \epsilon^2}-\frac{U}{\epsilon^2}+\frac{\partial^2 U}{\partial \eta^2} \tag{2}$$

$$\frac{\partial V}{\partial \tau}+U\frac{\partial V}{\partial \epsilon}+V\frac{\partial V}{\partial \eta}=Gr\theta-\frac{\partial P^*}{\partial \eta}+\frac{\partial^2 V}{\partial \epsilon^2}+\frac{1}{\epsilon}\frac{\partial V}{\partial \epsilon}+\frac{\partial^2 V}{\partial \eta^2} \tag{3}$$

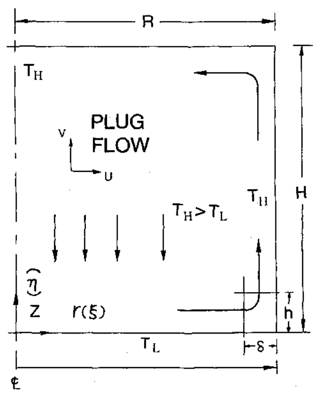

Fig. 1 Physical geometry of the present system.

$$\frac{\partial \theta}{\partial \tau}+U\frac{\partial \theta}{\partial \epsilon}+V\frac{\partial \theta}{\partial \eta}=\frac{1}{Pr}\left(\frac{\partial^2 \theta}{\partial \epsilon^2}+\frac{1}{\epsilon}\frac{\partial \theta}{\partial \epsilon}+\frac{\partial^2 \theta}{\partial \eta^2}\right) \tag{4}$$

All boundaries are considered to be rigid, i.e., $U=V=0$ (for $\tau \geq 0$), and the top and side walls are maintained at a temperature T_H, while the bottom wall is maintained at a temperature T_L as time goes on. Here, T_L is assumed to be less than T_H. It can be seen that there are three governing parameters in the problem at steady state: the Rayleigh number Ra, the aspect ratio (H/R), and the Prandtl number Pr.

A steady-state scale analysis might be drawn from Fig. 1. One can infer that the driving force is mainly caused by the buoyancy term and, therefore, the viscous force can be neglected. This gives the balance between the inertia term and buoyancy force in the momentum equation

$$v\frac{v}{h}\sim g\beta\Delta T \tag{5}$$

If we assume that

$$\delta\sim\Delta \tag{6}$$

for natural convection, the energy balance may be written as

$$v\frac{\Delta T}{h}\sim\alpha\frac{\Delta T}{\delta^2} \tag{7}$$

Here, h is the height of the boundary layer, whereas δ and Δ, respectively, stand for velocity and temperature boundary thickness.

As has been shown in the literature,[10] this is true with a Prandtl number of order unity or greater. Solving V from the foregoing equation

$$v\sim\frac{\alpha h}{\delta^2} \tag{8}$$

and inserting this velocity into Eq. (5) yield

$$\frac{h}{\delta}\sim\left(\frac{h}{R}\right)^{3/4}Ra^{1/4}Pr^{1/4} \tag{9}$$

The average Nusselt number on the side wall, in view of $\delta\sim\Delta$, is

$$\overline{Nu_s}\sim\frac{(Q/A/\Delta T)R}{K} \tag{10}$$

where

$$Q\sim K\left(\frac{\Delta T}{\delta}\right)2\pi Rh \tag{11}$$

and $A=2\pi RH$, with A denoting the surface area of the cylinder and K the thermal conductivity of the fluid.

Therefore, Eq. (9) becomes

$$\overline{Nu_s}\sim\left(\frac{H}{R}\right)^{-1}\left(\frac{h}{R}\right)^{3/4}Ra^{1/4}Pr^{1/4} \tag{12}$$

if we assume the scale of h is proportional to that of R. This analysis concludes with

$$\overline{Nu_s}\sim\left(\frac{H}{R}\right)^{-1}Ra^{1/4}Pr^{1/4} \tag{13}$$

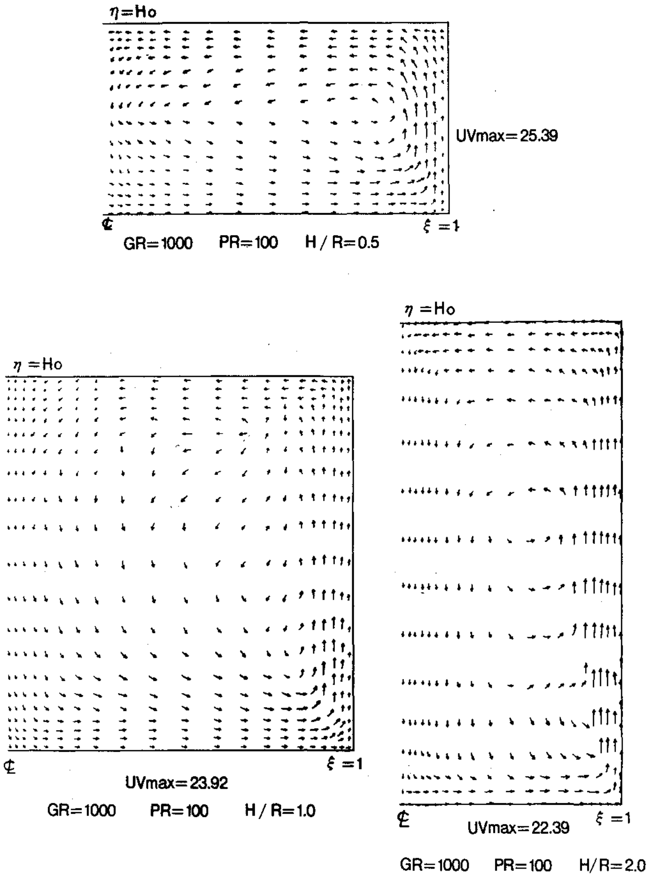

Fig. 2 Represenative velocity field for $Ra = 10^5$, $H/R = 0.5$, 1 and 2, respectively.

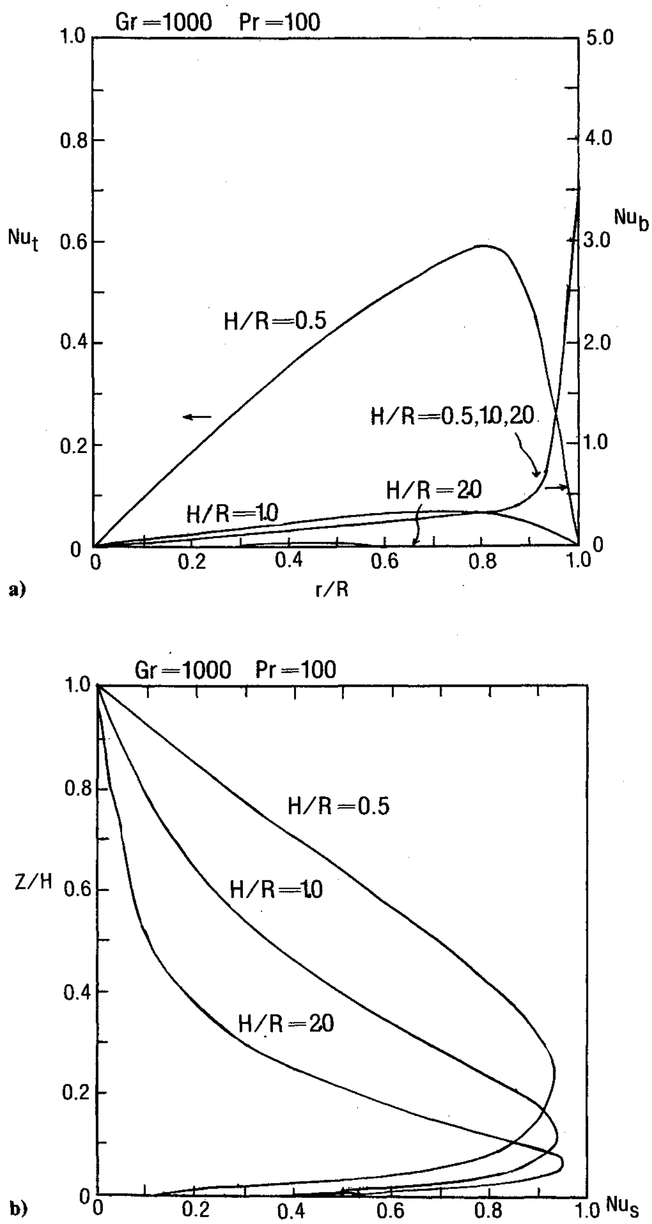

Fig. 3 The plots of Nu_t, Nu_b vs r/R and Nu_s vs Z/H.

Results and Discussion

At each time step ($\Delta\tau = 5 \times 10^{-3}$), the governing partial differential equations are solved using a control-volume-based finite-difference procedure called SIMPLE/HD.[11] The grid system, calculation procedure, and grid dependence examination were detailed in the work of Huang and Hsieh.[8] The result reported here corresponds to a steady-state solution. This solution was obtained following the criterion given by Wilkes and Churchill[12] for each time step. Results are presented for the values of Ra covering the range 1.0×10^4 to 1.0×10^6 for values of H/R of 0.5, 1, and 2 for Prandtl numbera of 1, 10, 100, and 200. Figure 2 shows a sequence of representative flow patterns calculated for the case of $Pr = 100$ for $Gr = 10^3$ with aspect ratios (H/R) of 0.5, 1, and 2, in which they all exhibit unicellular motion of the doughnut type. The common flow characteristic of these figures indicates that the flow is clearly driven by the differentially heated corner temperatures ($\sim\Delta T$) and becomes more and more localized as the aspect ratio (H/R) and Gr increase. The vertical jet accelerated in the vertical boundary-layer region discharges into a pool of nearly isothermal trapped fluid, and it decelerates and loses much of its flow rate before smoothly rounding the upper right-hand corner of the enclosures. This last characteristic becomes more visible as the H/R increases, because in this process the vertical boundary-layer region that drives the flow becomes short with respect to the height of the isothermal pool (H) that serves as a brake for the vertical jet flow originating from the corners. Moreover, it appears that the Prandtl number has less influence on the flow pattern than the aspect ratio and Grashof number, due to the larger movement of the center of the cat's eye-like vortex to the corner for different aspect ratios and Grashof numbers.

Figure 3a shows the local Nusselt number distribution based on the top ceiling and bottom floor along the radial axis with three aspect ratios. For the top ceiling the local Nusselt number increases to a certain value, then decreases to a lower value as r increases to the side wall boundary for all aspect ratios. This indicates that somewhere close to the side wall the heat transfer is quite high. This peak is toward the side wall, and its magnitude becomes higher as H/R decreases. Foo the bottom wall the local Nusselt number variation monotonically increases as r increases to the boundary and no aspect ratio effect is seen. This is perhaps due to the fact that the same horizontal boundary-layer thickness exists for the three aspect ratios.

The variation of the local Nusselt number on the hot side wall Nu_s, with z/H for three different aspect ratios, is shown in Fig. 3b. For all of the cases, convection increases Nu over most of the height of the enclosure. The maximum occurs near the bottom of the wall. This is to be expected since the fluid there just passed over the cold bottom wall, so the temperature gradients are greatest. As the fluid rises up along the hot side wall, its temperature rises and the heat transfer decreases. As the aspect ratio increases, the convective effect promotes greater heat-transfer rates for most of the height of the enclosure.

The average Nusselt number for the side wall is calculated according to the definition indicated in Huang and Hsieh.[8] It was suggested by Arpaci and Larsen[10] that the present $\overline{Nu_s}$ be represented in the form of

$$\overline{Nu_s} = 0.77(Ra)^{0.212}(Pr)^{0.291}(H/R)^{0.9}$$

for

$$0.5 \le (H/R)2.0$$

$$10^4 \le Ra \le 10^6$$

$$100 \le Pr \le 200 \tag{14}$$

to approximate the computed data within ±5% by least-squares curve fitting. It appears that this approximation agrees quite well with the results reported by Arpaci and Larsen[10] based on the two-length natural convection model and the scale analysis of the present configurations $\overline{Nu_s} \sim (H/R)^{-1}\ R^{0.25}\ Pr^{0.25}$). This indicates that the heat-transfer model used in the scale analysis accurately reflects the phenomenon inside the cylindrical enclosures.

Acknowledgment

The author wishes to express his appreciation to D. Y. Huang for early assistance with this paper and W. S. Han for the scale analysis.

References

[1]Edwards, D. K. and Catton, I., "Prediction of Heat Transfer by Natural Convection in Closed Cylinders Heated from Below," *International Journal of Heat and Mass Transfer*, Vol.12, No. 1, 1969, pp. 23–30.

[2]Liang, S. F., Vidal, A., and Acrivos, A., "Buoyance Driven Convection in Cylindrical Geometries," *Journal of Fluid Mechanics*, Vol. 36, No. 2, 1969, pp. 239–256.

[3]Rosenblat, S., "Thermal Convection in a Vertical Circular Cylinder," *Journal of Fluid Mechanics*, Vol. 122, No. 2, 1982, pp. 395–405.

[4]Verhoeven, J. D., "Experimental Study of Thermal Convection in a Vertical Cylinder of Mercury Heated from Below," *Physics of Fluids*, Vol. 12, No. 9, 1969, pp. 1733–1743.

[5]Yin, S. H., Lay, J. Y., and Hwang, J., "Natural Convection Heat Transfer in Vertical Cylindrical Enclosures," *Proceedings of National Science Council Monthly*, Vol. 2, No. 4, 1979, pp. 424–430.

[6]Huang, D. Y., "Buoyancy Driven Convection Within a Vertical Cylindrical Enclosure; Prandtl Number Effect," MS thesis, Dept. of Mechanical Engineering, National Taiwan Univ., Taipei, China, 1979.

[7]Kimura, S. and Bejan, A., "Natural Convection in a Differentially Heated Corner Region," *Physics of Fluids*, Vol. 28, No. 10, 1985, pp. 2980–2989.

[8]Huang, D. Y. and Hsieh, S. S., "Analysis of Natural Convection in a Cylindrical Enclosure," *Numerical Heat Transfer*, Vol. 12, No. 1, 1987, pp. 121–135.

[9]Figliola, R. S., "Convection Transitions Within a Vertical Cylinder Heated Flow Below," *Physics of Fluids*, Vol. 29, No. 9, 1986, pp. 2028–2031.

[10]Arpaci, V. S. and Larsen, P. S., *Convection Heat Transfer*, Prentice-Hall, Englewood Cliffs, NJ, 1984.

[11]Patankar, P. S., *Numerical Heat Transfer and Fluid Flow*, Hemisphere, New York, 1980.

[12]Wilkes, J. O. and Churchill, S. W., "The Finite-Difference Computation of Natural Convection in a Rectangular Enclosure," *AIChE Journal*, Vol. 12, No. 1, 1966, pp. 161–166.

Evaluation of Transport Conditions During Physical Vapor Transport Growth of Opto-Electronic Crystals

N. B. Singh* and R. Mazelsky†
Westinghouse R&D Center, Pittsburgh, Pennsylvania
and
M. E. Glicksman‡
Rensselaer Polytechnic Institute, Troy, New York

Nomenclature

a	= radius of growth tube, cm
c	= cold zone
D	= diffusion coefficient, cm^2/S
H	= hot zone
J	= mass flux, $moles/cm^2.S$
L	= transport length, cm
M	= molecular weight, g/mole
N_e	= dimensionless Peclet number
P	= vapor pressure, Torr
$\hat{P}$	= average pressure, Torr
R	= gas constant, atm/mole K
T	= temperature, K
$\hat{T}$	= average temperature, K
v	= growth velocity, cm/S
Ω	= molar volume, cm^3

Introduction

MERCUROUS halides show great promise for acousto-optic devices applied to signal-processing and optical spectrum-analyzing systems, and have attractive properties for high-performance devices. These halides have 1) a large transmission range, 2) high acousto-optic figure of merit, 3) suitable photoelastic coefficients, and 4) very slow acoustic velocity. During the last few years, we have investigated[1–4] growth anisotropy, the effect of growth parameters on optical quality, and the effect of crystal quality on the fabrication and characteristics of mercurous chloride acousto-optic devices. The crystals have been grown in closed tubes by the physical vapor transport (PVT) method. In the ongoing investigation of PVT crystal growth, we are studying the effect of thermal and solutal convection during vapor transport. This Note reports the effect of source temperature on mass flow and the growth rate.

Experimental

Purification of Source Material

The as-supplied source material was listed at 99+% purity. It was sublimed several times in a hermetically sealed tube until water-white material was achieved. The purity was checked by spark-source spectrometry. Source material contains less than 15 ppm total metallic impurities.

Presented as Paper 89-0229 at the AIAA 27th Aerospace Sciences Meeting, Reno, NV, Jan. 9–12, 1989; received Feb. 6, 1989; revision received April 4, 1989.

*Fellow Engineer, Department of Crystal Growth and Superconductor Research.

†Manager, Department of Crystal Growth and Superconductor Research.

‡John T. Horton Professor.